





Three-dimensional phase separation under a nonstationary temperature field

Rikuya Ishikawa , Marie Tani , and Rei Kurita 

Department of Physics, Tokyo Metropolitan University, 1-1 Minamioosawa, Hachioji-shi, Tokyo 192-0397, Japan

 (Received 25 January 2022; revised 11 May 2022; accepted 12 August 2022; published 26 August 2022)

Pattern formation via nonequilibrium dynamical paths has been the focus of much recent attention. An example is phase separation under the action of a nonstationary temperature field. Under directional quenching (DQ), where a region at some “quenched” temperature spreads in one direction over time, it has been found that a variety of patterns (random droplet, lamellar, and columnar patterns) may be formed by controlling the dynamics of the quenching front in two dimensions. Although a similarly rich phenomenology may be expected in three dimensions (3D), DQ in 3D would require temperature control in bulk, which is difficult to realize. Instead of DQ, we fix the temperature gradient through the slab, and control of the surface temperature of both sides of the slab (gradient cooling, GC). It seems similar to DQ and it is significantly easier to realize experimentally. Here, we compare the mechanism of the phase separation in DQ with that in GC. It is found that no columnar pattern is formed in GC. It is also revealed that a pattern formation mechanism in GC is clearly different from conventional DQ.

DOI: [10.1103/PhysRevResearch.4.033152](https://doi.org/10.1103/PhysRevResearch.4.033152)

I. INTRODUCTION

Phase separation may occur when a well-mixed binary system such as a metal alloy or liquid mixture is quenched. As the phase separation proceeds, a droplet pattern or a bi-continuous pattern is formed [1–11]. The patterns are related to macroscopic properties such as mechanical properties [12], electrical conductivity [13], and thermal conductivity [14]. There have also been many attempts to control pattern formation during phase separation. Examples include double quenching with two temperature quenches [15], manipulation of the wettability of the surface on which a system is mounted [16,17], phase separation under a temperature gradient [18], and pattern formation making use of colloidal inclusions, using both the wettability of the liquid-colloid interface and the mobility of the colloids themselves [19,20]. Recently, pattern formation using directional quenching (DQ) in two dimensions (2D), where a quenched region spreads in one direction, has attracted much attention [21–25]. It is worth noting that the temperature field in DQ is heterogeneous, but finally becomes homogeneous, the same as the final state of a homogeneous quench, i.e., DQ gives rise to phase separation via a different dynamical path with the same destination. It has been reported that three types of patterns are produced in 2D depending on the speed V of the quenching front separating low- and high-temperature regions: a random droplet and lamellar and columnar (or laterally oriented lamellar) patterns [21–23]. Recently, we revealed that the transition between lamellar and columnar patterns is caused

by an effective confinement effect produced by the quenching front [25].

However, DQ is an idealized quenching method, since it requires control over the internal temperature of a bulk sample. Nevertheless, the parameter dependent formation of a random droplet, lamellar, and columnar patterns are widely observed in systems mirroring the idea of DQ, for example, the aggregation of colloids under radially propagating fronts [26], phase separation due to temperature gradients formed around colloids [27,28], recrystallization in sodium chloride solution on substrates [29,30], and pattern formation due to phase separation in films and collagen networks [31,32]. In metallic alloys, eutectic patterns have been observed to self-assemble perpendicular to the crystal-growth direction when it solidifies in a certain direction [33–35]. These methods are called directional solidification or directional ordering [36]. Rich phenomenology of pattern formations were also observed in liquid crystals and binary alloys using directional ordering [37,38]. Such patterns are similar to the columnar patterns seen in DQ, suggesting a link between directional solidification and DQ.

The experimental realization of DQ in a three-dimensional block of material may be quite difficult. Instead of DQ, cooling via an adjacent surface may be considered as an alternative method. For example, by tuning the temperature of both sides of a slab of material, we may fix the temperature gradient across the block; by reducing the temperature of both sides at the same rate, the gradient is preserved while the system is driven to quench from one side to the other. We call this gradient cooling (GC). In this work, we undertook a systematic comparison of DQ and GC. It is found that the columnar patterns of the majority phase seen under DQ are no longer realized under GC. Although the difference may seem subtle, we found through numerical simulation that the pattern formation mechanism in conventional DQ and GC is qualitatively distinct.

Published by the American Physical Society under the terms of the Creative Commons Attribution 4.0 International license. Further distribution of this work must maintain attribution to the author(s) and the published article's title, journal citation, and DOI.

II. METHOD

The dynamics of phase separation under homogeneous quenching is described by the Cahn-Hilliard-Cook equation [1,4,39]. A modified-Cahn-Hilliard-Cook equation was proposed for systems with a temperature gradient. This equation takes account of the concentration transport due to the temperature gradient [40]. Since the concentration transport by a temperature gradient is proportional to $\Delta T/T$, it can be neglected when the quench is shallow i.e., the temperature gradient term (Ludwig-Soret effect) is neglected. Here, we normalize length and time using a correlation length and characteristic time at an initial temperature; we normalize the concentration ϕ by the concentration after phase separation. The normalized equations are given as

$$\frac{\partial \phi}{\partial t} = \nabla^2 [\epsilon(\vec{r}, t)\phi + \phi^3 - \nabla^2 \phi] - \vec{\nabla} \cdot \vec{g}(\vec{r}, t), \quad (1)$$

where ϕ , \vec{r} , and t are normalized concentration, normalized position, and normalized time, respectively. A normalized temperature $\epsilon(\vec{r})$ is defined as $\epsilon(\vec{r}, t) = [T(\vec{r}, t) - T_c]/(T_0 - T_c)$, where T_0 and T_c are the initial temperature and the critical temperature, respectively. When $\epsilon > 0$, the mixed state becomes stable; when $\epsilon < 0$, phase separation occurs. Assuming local equilibrium and applying the fluctuation-dissipation relation, the correlation function of the dimensionless noise $\vec{g}(\vec{r}, t)$ can be described as

$$\langle \vec{g}_i(\vec{r}, t) \vec{g}_j(\vec{r}', t') \rangle = \Theta(\vec{r}) \delta_{ij} \delta(\vec{r} - \vec{r}') \delta(t - t'), \quad (2)$$

where $i, j = x, y, z$ and $\Theta(\vec{r})$ corresponds to fluctuation strength. Although $\Theta(\vec{r})$ is proportional to $T(\vec{r})$, $\Theta(\vec{r})$ can be regarded as constant since the term $\Delta T/T(\vec{r})$ can be neglected at any \vec{r} . Then we set $\Theta(\vec{r}) = 0.001$ at any \vec{r} , which corresponds to a noise amplitude at $T(\vec{r}) = T_0$. Here we note that the thermal noise is given as perturbation for the instability of the interface, and then the pattern formation is insensitive for the value of $\Theta(\vec{r})$.

Due to the apparent difference in the temperature profiles, we refer to the system with phase separation driven by three-dimensional DQ as the discontinuous system, and the system with a fixed temperature gradient, i.e., the GC system as the continuous system. To distinguish between the temperatures of two systems, we denote the temperature in the discontinuous system as ϵ_d and the temperature in the continuous system as ϵ_c . Figure 1 shows the time evolution of the temperature field for both ϵ_d and ϵ_c . The temperature ϵ_d of the discontinuous system is set to

$$\epsilon_d(z, t) = \begin{cases} 1 & z > V_d t \\ -1 & z \leq V_d t \end{cases}, \quad z \in [0, L_z], \quad (3)$$

where V_d is the speed of the quenching front in the discontinuous system, and L_z is the system size in the z direction [see Fig. 1(a)]. Meanwhile, the temperature ϵ_c of the continuous system is set to

$$\epsilon_c(z, t) = \max\left(\frac{z - V_c t}{L_z}, -1\right), \quad z \in [0, L_z], \quad (4)$$

where V_c is the speed at which the isothermal surface where $\epsilon_c = 0$ moves in the continuous system [see Fig. 1(b)]. One can see that there is a correspondence between the isothermal

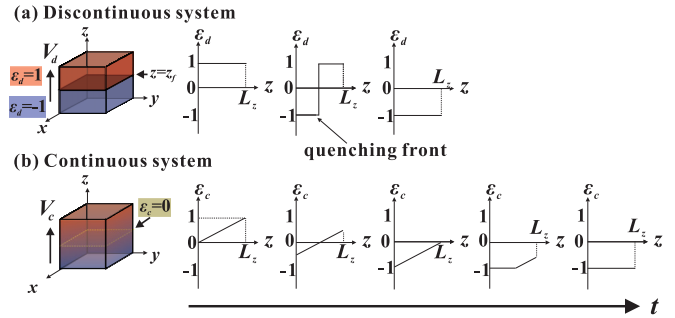


FIG. 1. Time evolution of the temperature in the two systems. (a) In the discontinuous system, the boundary between $\epsilon_d = -1$ and $\epsilon_d = 1$ (quenching front, $z = z_f$) moves with a constant velocity V_d from the bottom of the z axis at $t = 0$. (b) In the continuous system, the linear temperature gradient is applied in the z direction, and the temperatures at the top and bottom surfaces are quenched at the same rate. The isothermal line where $\epsilon_c = 0$ moves with constant velocity V_c .

surface where $\epsilon_c = 0$ and the quenching front of the discontinuous system. In an experiment, V_c can be controlled by tuning the rate at which the temperature of the top and bottom surfaces is quenched. Finally, the temperature becomes homogeneous as $\epsilon = -1$ in both systems.

We note that the diffusion of the temperature can be described as

$$\frac{\partial \epsilon}{\partial t} = Le \nabla^2 \epsilon, \quad (5)$$

where $Le = \frac{K}{L}$ is Lewis number, K is the thermal diffusion coefficient, and L is the concentration diffusion coefficient. In a real system, K is about 10^{-4} m²/s in metal and 10^{-7} m²/s in water, while L is about 10^{-12} m²/s in metal and 10^{-9} m²/s in water. Thus, Le is about 10^8 in a metallic system and 100 in a water system. Since Le is quite large, the temperature can be considered in equilibrium in a usual system. That is why the temperature field is input as an equilibrium state instead that we simulate the temperature field by the thermal diffusion equation.

In this simulation, we set $\Theta = 0.001$ for all \vec{r} . We used periodic boundary conditions in the xz and yz planes, and set a free surface in the xy plane. The system size is $L_x : L_y : L_z = 128 : 128 : 128$. Hydrodynamic interactions were neglected. The effect of latent heat was also neglected. The initial concentration field is set to be asymmetric, with an average concentration of $\bar{\phi} = 0.1$. First, we annealed the whole system for a long time at $\epsilon(\vec{r}) = 1$ for the discontinuous system, and $\epsilon(z) = z/L_z$ for the continuous system. DQ or GC is then initiated at $t = 0$. All simulations were repeated five times starting from different initial states. The data and error bars shown are the mean and standard deviations over the five runs.

III. RESULTS

A. Pattern formation

First, we study the V dependence of the pattern formation during phase separation in the discontinuous and continuous systems. The pattern is classified when the top surface is

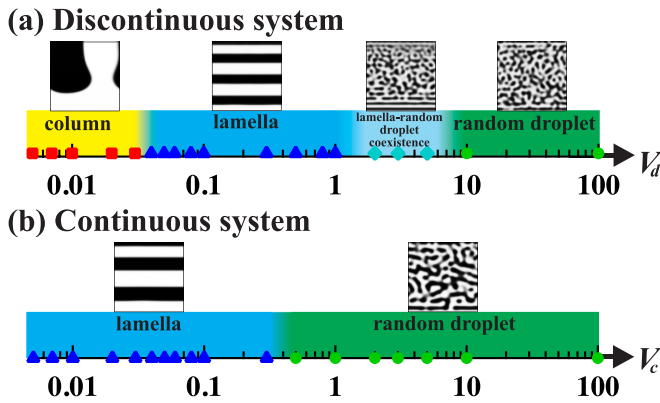


FIG. 2. Patterns at different V . The pattern is classified when the top surface is quenched below $\epsilon = 0$. Symbols correspond to points simulated. Circles, diamonds, triangles, and squares correspond to random droplet, random droplet-lamellar coexistence, lamellar, and columnar patterns, respectively. Panel (a) is for the discontinuous system, and panel (b) is for the continuous system.

quenched below $\epsilon = 0$. Figures 2(a) and 2(b) show what patterns are found at different front velocities. White and black in the patterns correspond to the majority and minority phases, respectively. In the discontinuous system, columnar, lamellar, and random droplet patterns are formed as V_d is increased, just like in two-dimensional DQ [21,25]. On the other hand, in the continuous system, lamellar and random droplet patterns are formed, but no columnar pattern is formed at least for $V_c \geq 0.005$ (each pattern is also shown in Fig. 3).

Next, we show the time evolution of the patterns in the discontinuous system. Figure 3(a1) shows the time evolution of the xz section of the droplet pattern for the discontinuous system when $V_d = 10$ ($y = L_y/2$) at $t = 130, 500$, and 1000 from left to right. Figure 3(a2) shows the xy section of the pattern ($z = L_z/2$) at $t = 1000$. The speed of the front V_d is faster than the dynamics of phase separation; a random droplet pattern is thus formed just like for homogeneous quenching. Figure 3(b1) shows lamellar pattern formation in the xz section when $V_d = 0.05$ ($y = L_y/2$) at $t = 200, 1400$, and 4000 . Figure 3(b2) shows the pattern in the xy section ($z = L_z/2$) at $t = 4000$. It is clear that the concentration is homogeneous in the xy section, confirming the lamellar structure. At an early stage, the majority phase appears as a layer on the bottom surface, since $\bar{\phi} = 0.1$. A layer of the minority phase subsequently appears above the emerged majority layer. This process alternates to create a lamellar pattern. Figure 3(c1) shows an xz section of the pattern ($y = L_y/2$) when $V_d = 0.007$ at $t = 3600, 9600$, and $19\,500$. Again, the majority phase initially appears as a layer on the bottom surface. However, unlike in the case of the lamellar pattern, the minority phase appears perpendicular to the layer of the majority phase. Figure 3(c2) shows an xy section ($z = L_z/2$) at $t = 19\,500$. It is found that the majority phase has a cylindrical shape, and the minority phase forms a background matrix. Here we note that the interface between the majority and minority phases is flat in two-dimensional DQ and the lamellar pattern geometrically equivalent to the columnar pattern [25]. However, in three-dimensional DQ, a geometric distinction (curvature) emerges between the two phases due to an

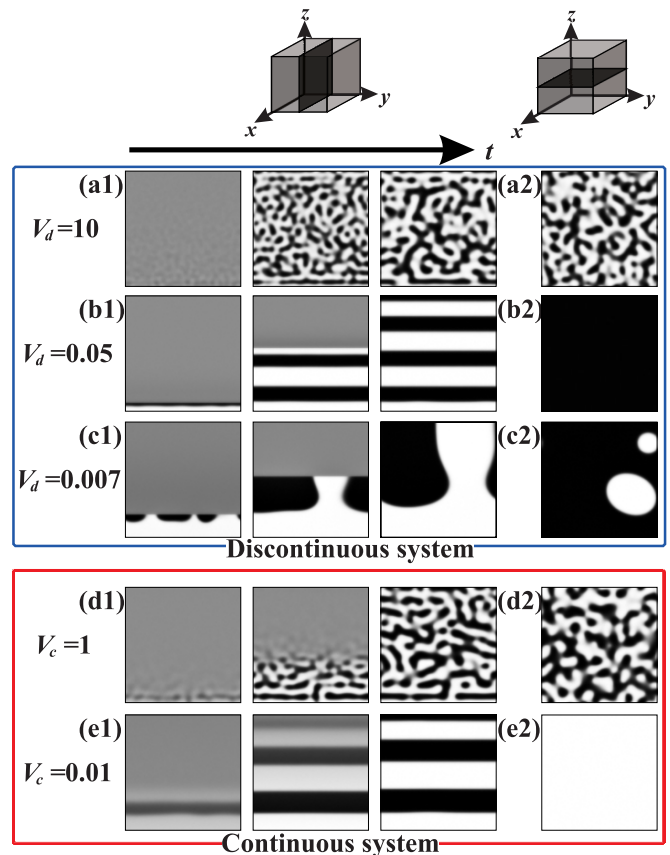


FIG. 3. Time evolution of the patterns during phase separation. Panels (a)–(c) correspond to the discontinuous system and panels (d)–(e) correspond to the continuous system. Panels (1) correspond to the xz section at $y = L_y/2$. Panels (2) correspond to xy section at $z = L_z/2$ at the same time when the right image of panels (1), respectively. (a) Random droplet pattern when $V_d = 10$ at $t = 130, 500$, and 1000 . (b) Lamellar pattern when $V_d = 0.05$ at $t = 200, 1400$, and 4000 . (c) Columnar pattern when $V_d = 0.007$ at $t = 3600, 9600$, and $19\,500$. (d) Random droplet pattern when $V_c = 1$ at $t = 100, 150$, and 256 . (e) Lamellar pattern in the xy plane ($y = L_y/2$) when $V_c = 0.01$ at $t = 5000, 12\,800$, and $25\,600$. The lamellar pattern becomes clear gradually over time in panel (e): this is different from pattern evolution in the discontinuous system. In addition, a columnar pattern is not formed in the continuous system at least when $V_c \geq 0.005$.

increase of dimension. This geometric difference ultimately leads to a significant difference in the coarsening process (see section D). In addition, we also note that the formation of a background matrix of the minority phase is in itself different from what is seen during phase separation in homogeneous quenching.

Next, we look at time evolution of the patterns in the continuous system. Figure 3(d1) shows an xz section ($y = L_y/2$) of the pattern when $V_c = 1$ at $t = 100, 150$, and 256 from left to right. Figure 3(d2) shows an xy section ($z = L_z/2$) of the same pattern at $t = 256$. Since the phase separation cannot keep up with the temperature change, a random droplet pattern is formed, much like the discontinuous system. Figure 3(e1) shows an xz section ($y = L_y/2$) of the pattern when $V_c = 0.01$ at $t = 5000, 12\,800$, and $25\,600$. Figure 3(e2) shows an xy

section ($z = L_z/2$) of the same pattern when $t = 25\,600$. It is confirmed that a lamellar pattern is formed when $V_c = 0.01$. However, we note that the lamellar pattern only becomes gradually clear over time: this is different from pattern evolution in the discontinuous system.

B. Stability of the lamellar pattern in the discontinuous system

Here, we investigate the mechanism behind columnar pattern formation in the discontinuous system. In two-dimensional DQ, the majority layer appears first, followed by fluctuations at its interface [25]. We note that the analysis for the fluctuations at the interface in 3D is statistically more reliable than that in 2D. When the fluctuations are large enough to be stable, a columnar pattern is formed. It was also reported that the fluctuations become large when the distance between the interface and the quenching front is short. In three-dimensional DQ, the interface of the first majority layer is a two-dimensional plane, making it suitable for a more quantitative analysis. To quantitatively evaluate the concentration fluctuations at each z , we define the concentration variance $\sigma(z, t)$ by the following formula:

$$\sigma(z, t) = \frac{\int dx dy [\phi(x, y, z, t) - \langle \phi(z, t) \rangle_{x,y}]^2}{L_x L_y}, \quad (6)$$

where

$$\langle \phi(z, t) \rangle_{x,y} = \frac{\int dx dy \phi(x, y, z, t)}{L_x L_y}. \quad (7)$$

When $\sigma(z, t)$ is zero, the concentration field is uniform in the xy plane.

Figure 4(a) shows $\sigma(z, t)$ as a function of z and t when $V_d = 0.04$ in the discontinuous system. When $V_d = 0.04$, a lamellar pattern is formed. Note that darker regions correspond to larger $\sigma(z, t)$. $\sigma(z, t)$ shows a peak when a new layer is formed [see inset in Fig. 4(a)], suggesting that it corresponds to interfacial fluctuations. Here, we define $z_m(t)$ as the position where $\sigma(z, t)$ is largest at t ; we confirm that $z_m(t)$ corresponds to the position of the interface between the layers. We also define $t = \tau$ as the time at which $\sigma(z_m, t)$ is maximized. Here, we define τ_0 as a time when the interface begins to fluctuate. Thus, $\tau - \tau_0$ is the time period for growing the fluctuations. Figure 4(b) shows that V_d dependence of $\tau - \tau_0$ in the discontinuous system. It is found that $\tau - \tau_0$ increases with decreasing V_d .

To clarify the origin of interfacial fluctuations, we also computed a structure factor $S(q)$ by Fourier transforming the concentration field in the plane at $z = z_m$ when $V_d = 0.04$ in the discontinuous system. It is found that $S(q)$ has a broad peak at $q = q_m = 6$; note that q_m remains almost constant between $t = 190$ and 240 [Fig. 5(a)]. In addition, the peak intensity $S(q_m)$ increases exponentially over time at early times [Fig. 5(b)]. These features are the same as what is expected in the Cahn linear regime during spinodal decomposition [4]. Thus, this suggests that the interfacial fluctuations may be related to spinodal decomposition. We note that the correlation length of interfacial fluctuations in this system is $L_x/q_m \approx 21$. It is different from the correlation length in ordinal spinodal decomposition (≈ 13 obtained by homogeneous quenching in 2D). In DQ, the concentration field in the z direc-

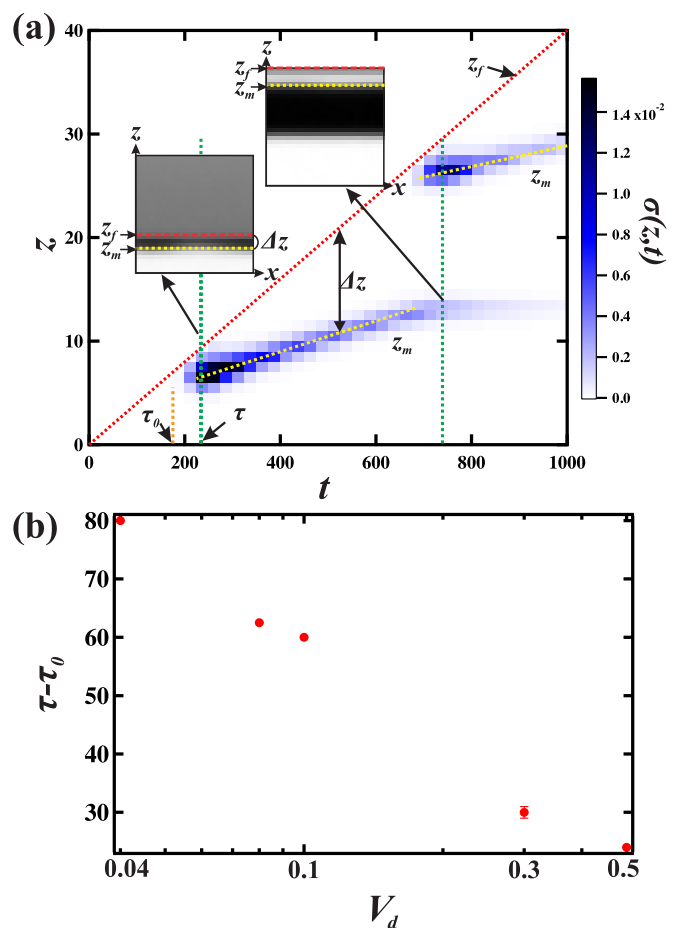


FIG. 4. (a) $\sigma(z, t)$ when $V_d = 0.04$ in the discontinuous system. Darker regions correspond to larger $\sigma(z, t)$. The red dashed line shows the position of the quenching front [$z = z_f(t)$]; the yellow dashed line shows the position of the interface between layers [$z = z_m(t)$]. The insets are the patterns at $y = L_y/2$ at the times indicated by green dashed lines, enlarged over the area enclosed by $(x, z) = (0, 0) - (30, 30)$. (b) V_d dependence of $\tau - \tau_0$ in the discontinuous system. $\tau - \tau_0$ increases with decreasing V_d .

tion is inhomogeneous, affecting the spinodal decomposition at the interface. We note that any further theoretical discussion is difficult since a linear stability analysis would be required for nonsteady, heterogeneous systems. It was reported that the lamellar pattern is again formed for much smaller $V \approx 10^{-4}$ in Ref. [23]. It means that the system cannot be regarded as steady state even though $V = 0.005$.

Next, we show how V_d depends on $\sigma(z_m, \tau)$ in a range where lamellar patterns are formed. The triangles in Fig. 6 correspond to $\sigma(z_m, \tau)$ in the discontinuous system. It is found that $\sigma(z_m, \tau)$ is large not only near the boundary between random droplets and lamellae, but also near the boundary between lamellae and columns. This suggests that the stability of the lamellar pattern is affected by V_d .

Here, we consider the stability of the lamellar pattern. Because of the asymmetric initial concentration ($\bar{\phi} = 0.1$), a layer of the majority phase is initially formed at the base. It is expected that the layer is stable when the flux in the z direction j_z is much larger than the flux in the x direc-

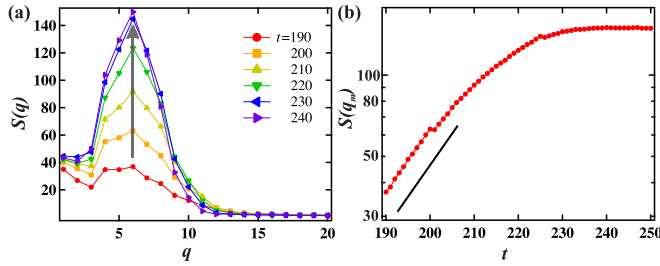


FIG. 5. Structure factor of interfacial fluctuations when $V_d = 0.04$ in the discontinuous system. (a) $S(q)$ has a peak at wavelength $q_m = 6$ and $S(q_m)$ grows with time. (b) $S(q_m)$ increases exponentially over time at earlier stages, as shown by the solid line. This suggests that the growth of interfacial fluctuations is related to spinodal decomposition.

tion j_x or y direction j_y . We investigated how the flux near the interface depends on V_d . We computed the flux using $j_i = \nabla_i[\epsilon\phi + \phi^3 - \nabla^2\phi]$, where $i = x, y, z$. Furthermore, we defined a parameter γ as follows:

$$\gamma = \frac{\langle |j_x(z_m, \tau)| \rangle_{x,y} + \langle |j_y(z_m, \tau)| \rangle_{x,y}}{2\langle |j_z(z_m, \tau)| \rangle_{x,y}}, \quad (8)$$

where

$$\langle |j_i(z_m, \tau)| \rangle_{x,y} = \frac{\int dx dy |j_i(x, y, z_m, \tau)|}{L_x L_y}. \quad (9)$$

$\gamma < 1$ when the flux in the z direction is dominant, and vice versa. The circles in Fig. 7 show the V_d dependence of γ . We also show the distance $\Delta z(\tau) (=z_f - z_m)$ between the quenching front $z_f(\tau)$ and the interface position $z_m(\tau)$ at $t = \tau$. When $V_d \geq 2$, γ and $\sigma(z_m, \tau)$ increase with increasing V_d [also see Fig. 6]. Because of the large $\Delta z(\tau)$, the growth of the interface does not keep up with the migration of the quenching front. Thus, fluctuations grow above the interface or in bulk due to spinodal decomposition. Meanwhile, when $0.3 \leq V_d \leq 1$, γ is small and $\sigma(z_m, \tau)$ is also small. Therefore, it is confirmed

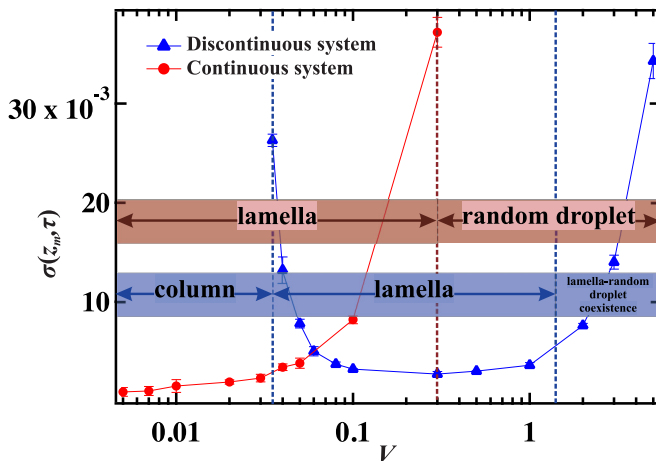


FIG. 6. V dependence of $\sigma(z_m, \tau)$. Triangles and circles correspond to $\sigma(z_m, \tau)$ in the discontinuous system and the continuous system, respectively. $\sigma(z_m, \tau)$ is large near the pattern boundaries. This suggests that the stability of the lamellar pattern is affected by V .

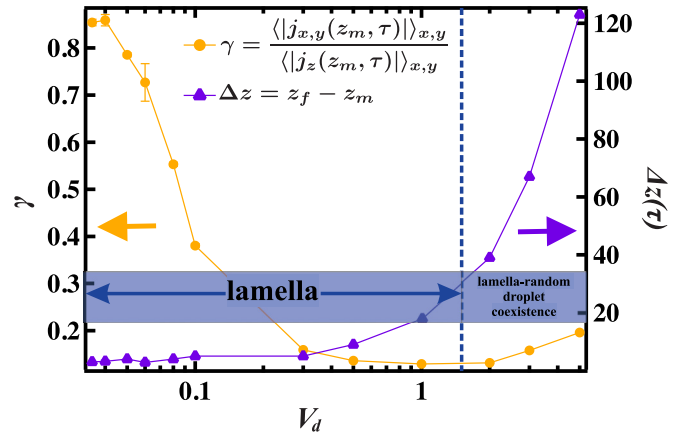


FIG. 7. V_d dependence of γ (circles) and $\Delta z(\tau)$ (triangles) in the discontinuous system. When $V_d \geq 2$, γ and Δz increase with increasing V_d . This indicates that fluctuations grow above the interface or in bulk due to spinodal decomposition. When $0.3 \leq V_d \leq 1$, γ is small and the lamellar pattern is stable. When $V_d \leq 0.2$, γ increases with decreasing V_d and $\Delta z(\tau)$. The effective confinement induced by the quenching front suppresses j_z , making the lamellar pattern unstable.

that the lamellar pattern is stable when the flux in the z direction is dominant. When $V_d \leq 0.2$, γ increases again with decreasing V_d and $\sigma(z_m, \tau)$ becomes larger. In this region, it is found that $\Delta z(\tau)$ is small. Since a mixed state is stable above $z = z_f$, concentration flow across the quenching front is not desirable; this means that j_z at $z = z_f$ is small. Therefore, the quenching front can be regarded as an effective boundary condition. This effective confinement becomes stronger when Δz is small, inducing a smaller j_z . As a result, γ becomes large, and the stability of the lamellar pattern decreases. When V_d is even smaller, the lamellar pattern finally becomes unstable and a columnar pattern is formed. This result is consistent with pattern formation in two-dimensional DQ [25], indicating that the mechanism behind pattern formation is independent of spatial dimensions.

C. Stability of the lamellar pattern in the continuous system

Next, we consider the stability of the lamellar pattern in the continuous system. Shown by the circles in Fig. 6, $\sigma(z_m, \tau)$ monotonically decreases with decreasing V_c in the continuous system. Since the interfacial fluctuations are small, columnar patterns are not formed in the continuous system at least for $V_c \geq 0.005$. To predict the pattern for $V_c < 0.005$, the difference between the pattern formation mechanism for DQ and GC needs to be clarified. Here, we consider the time evolution of the concentration profile in both systems. Figure 8 shows the time evolution of $\langle \phi(z, t) \rangle_{x,y}$ when $V = 0.1$ (lamellar patterns are formed in both systems) in Fig. 8(a) the discontinuous system and in Fig. 8(b) the continuous system. In the discontinuous system, the phase separation occurs such that layers form sequentially in the quenched region, reaching values of $\phi = \pm 1$; this means that a large concentration difference is formed near the interface. This causes a large j_z near the interface, which stabilizes the lamellar pattern. On the other hand, in the continuous system, a lamellar pattern is still formed, but the value of ϕ is not ± 1 . Instead, the

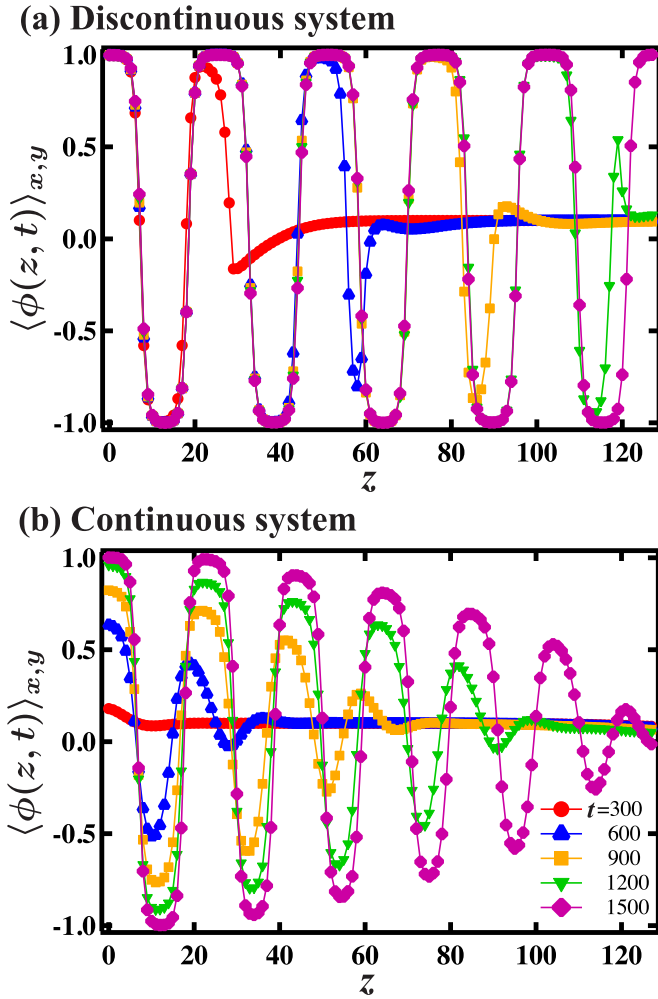


FIG. 8. Time evolution of $\langle \phi(z, t) \rangle_{x,y}$ when $V = 0.1$. (a) In the discontinuous system, layers of majority and minority phases form sequentially. (b) In the continuous system, lamellar patterns form in the entire quenched region, and the amplitude of $\langle \phi(z, t) \rangle_{x,y}$ gradually increases over time.

equilibrium concentrations are $\phi = \pm\sqrt{-\epsilon}$. The cooling in the GC case is not a deep quench near the surface of zero temperature. The pattern asymptotically approaches $\phi = \pm 1$ over time, together with the changing local temperature. Here we note that the flux in the continuous system is a few orders of magnitude smaller in all directions than in the discontinuous system, and that the system nearly reaches a steady state. In the continuous system, when V_c is small, the temperature changes slowly and a lamellar pattern is formed in the entire quenched region from an early stage. Therefore, it is expected that the lamellar pattern becomes stable with decreasing V_c , and that a columnar pattern is not formed in the continuous system even when $V_c < 0.005$.

D. Pattern formation and coarsening process

We investigate the pattern formation process of lamellar pattern at the early stage. We define η as the lamellar thickness at the bottom. We define the lamellar thickness as the length of the lowest region where $\langle \phi(z, t) \rangle_{x,y} > 0.5$. Figure 9 shows

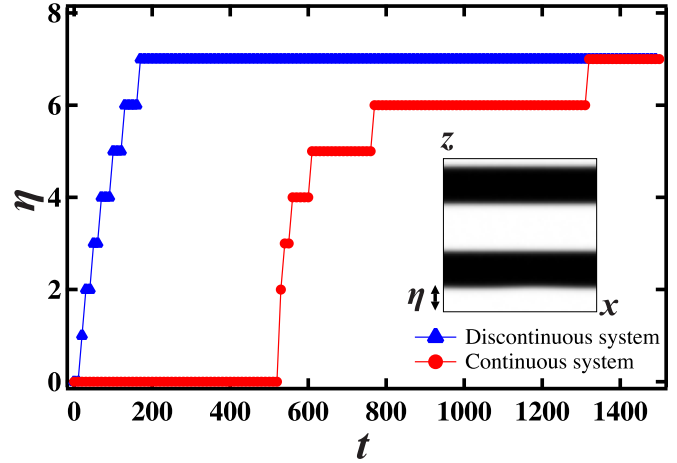


FIG. 9. Time evolution of η when $V = 0.1$. Triangles and circles correspond to η in the discontinuous system and in the continuous system, respectively. We define the lamellar thickness as the length of the lowest region where $\langle \phi(z, t) \rangle_{x,y} > 0.5$. In the discontinuous system, η saturates quickly. In contrast, in the continuous system, it takes a long time before η saturates.

the time evolution of η when $V = 0.1$. In the discontinuous system, η saturates quickly. In contrast, in the continuous system, it takes a long time before η saturates. This result is consistent with that ϕ in the continuous system gradually increases with time as shown in Fig. 8(b).

We also investigate the coarsening process of the patterns after the system is entirely quenched. The coarsening process is decided only by the structure, rather than by the quenching methods (DQ or GC). First, we investigate the coarsening of the lamellar pattern. No coarsening is observed in the lamellar pattern at later times since coarsening is fundamentally driven by curvature of the interface [4]; the interface is flat in the lamellar pattern. This is not the case for the columnar patterns which formed in the discontinuous system; it has curvature and therefore coarsens. As shown in Fig. 10(a), we define λ as the thickness of the majority phase layer formed at the bottom of the system, and ζ as the diameter of a column at $z = L_z/2$. Figure 10(b) shows the time evolution of λ and ζ for five independent runs. ζ is only given for times when the cross section of the column is circular. It is found that both λ and ζ increase with time. It suggests that a formed cylindrical pattern should be stable since the cylinder becomes wider with time. We also note that the system reaches an equilibrium state when λ is constant after a long time. The reason why the power varies from run to run largely could be that the small system size of this simulation plays a significant effect. It is expected that a simulation of a larger system will provide a more accurate estimate.

IV. DISCUSSION

Here we discuss the strength of the confinement effect in both discontinuous and continuous systems. In the discontinuous system, Fig. 8(a) shows that there is a clear separation between $\langle \phi(z, t) \rangle_{x,y} = 0.1$ in the high-temperature region ($\epsilon_d = 1$) and $\langle \phi(z, t) \rangle_{x,y} = \pm 1$ in the low-temperature region ($\epsilon_d = -1$). The quenching front has the effect of

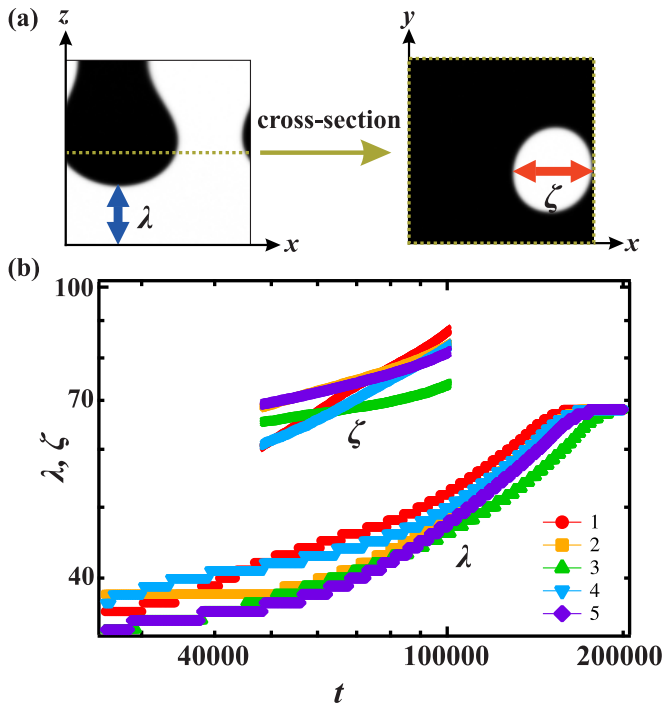


FIG. 10. (a) λ is the thickness of the majority phase layer formed at the bottom and ζ is a diameter of the column at $z = L_z/2$. (b) The time evolution of λ and ζ when $V_d = 0.005$ at a later stage for five runs. Both λ and ζ increase over time.

geometrically restricting the space (a finite-size effect) and suppressing the flux beyond the front (a boundary effect). When Δz is comparable to the droplet size where it is a few times larger than the correlation length in bulk ξ_0 (≈ 11 obtained by the homogeneous quenching in 3D) [see Fig. 7], the effective finite-size effect prevents the formation of a random droplet pattern, creating a lamellar pattern [41]. When Δz becomes even smaller (3–4 at $V_d = 0.05$), j_z is suppressed by the boundary effect of the quenching front, becoming comparable to j_x and j_y . We defined another correlation length ξ_d (3–4) where j_z becomes comparable to j_x and j_y . At this point, the lamellar pattern becomes unstable and transitions to a columnar pattern (Fig. 11).

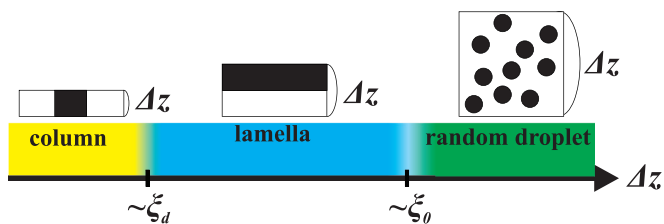


FIG. 11. Relation between the pattern diagram and Δz in the discontinuous system. When Δz is smaller than the droplet size which is a few times larger than the correlation length in bulk ξ_0 , the space is geometrically restricted, and then a lamellar pattern is formed. Furthermore, when Δz is smaller than the correlation length ξ_d , the flux in the z direction is suppressed and the layered pattern becomes unstable. Thus, a columnar pattern is formed.

In the continuous system, the space is geometrically restricted in the same way as in the discontinuous system since phase separation is restricted to the region where $\epsilon_c > 0$. Thus, a lamellar pattern is formed. However, the restoring force for the concentration difference is weak around the isothermal surface where $\epsilon_c = 0$; the flow through this surface is suppressed. That is, the isothermal surface where $\epsilon_c = 0$ cannot be regarded as a wall in any way. Therefore, the lamella structure is formed in the entire quenching region even at an early stage, preventing the formation of columnar patterns.

Next, we discuss the reason why interfacial fluctuations can occur but also decay over time during the formation of lamellae [see Fig. 4(a)]. The position of the interface z_m slowly increases when the interface is formed, while the position of the quenching front z_f changes significantly faster than z_m . Before $t = \tau$, Δz is temporarily smaller than ξ_d , allowing interfacial fluctuations to grow. A little later, Δz exceeds ξ_d , stabilizing the lamellar pattern. On the other hand, when V_d is too small and the time period over which $\Delta z < \xi_d$ is long, the fluctuations grow enough to form the columnar pattern [see Fig. 4(b)].

Finally, we compare our results with experiments looking at eutectic crystal growth in a temperature gradient. In the continuous system, no pattern perpendicular to the isothermal surface is formed. However, in eutectic experiments performed in the same way as in the continuous system, a pattern perpendicular to the isothermal surface has indeed been observed [33]. The eutectic system is different from the simple system considered in this simulation. Two order parameters are at least related in the eutectic system; a nonconserved order parameter, describing the liquid-solid transition, and the concentration, which is a conserved one, describing the transition between the two solids.

V. SUMMARY

We study three-dimensional phase separation patterns in two distinct systems, a discontinuous system with a step-like, moving quenching front, and in a continuous system where a constant-temperature gradient is maintained while the temperatures of both extremities of a sample are reduced at the same rate. Depending on the migration speed V of the quenching front and the isothermal surface where $\epsilon_c = 0$, three types of patterns (random droplet, lamellar, columnar patterns) are formed in the discontinuous system and two types of patterns (random droplet, lamellar patterns) are formed in the continuous system. It is expected that there are two characteristic lengths to determine the patterns (Fig. 11). When the effective confinement distance Δz is smaller than the correlation length in bulk ξ_0 , the space is geometrically restricted and a pattern parallel to the wall is formed. Meanwhile, when Δz is smaller than a distance ξ_d , where the flux in the z direction is suppressed such that it is comparable to the flux in the xy direction, a pattern perpendicular to the wall is formed. On the other hand, the isothermal surface where $\epsilon_c = 0$ cannot suppress the flux in the z direction in the continuous system, meaning that ξ_d do not exist and a columnar pattern cannot be formed in the continuous system. Thus, we conclude that the mechanism of pattern formation using a temperature gradient is significantly different from that by DQ. We hope that this

study will lead not only to the development of new physical understanding of pattern formation, but also be applied to the engineering of microscopic structures.

ACKNOWLEDGMENTS

M.T. was supported by JSPS KAKENHI (20K14431) and R.K. was supported by JSPS KAKENHI (20H01874).

-
- [1] J. W. Cahn and J. E. Hilliard, Free energy of a nonuniform system. i. interfacial free energy, *J. Chem. Phys.* **28**, 258 (1958).
- [2] Y. Tamura, M. Tani, and R. Kurita, Computationally Efficient Modeling of Ordering of Quenched Phases, *Phys. Rev. Lett.* **58**, 836 (1987).
- [3] S. Puri, Phase separation in an off-critical quench, *Phys. Lett. A* **134**, 205 (1988).
- [4] A. Onuki, *Phase Transition Dynamics* (Cambridge University Press, Cambridge, 2002).
- [5] H. Tanaka and T. Araki, Simulation Method of Colloidal Suspensions with Hydrodynamic Interactions: Fluid Particle Dynamics, *Phys. Rev. Lett.* **85**, 1338 (2000).
- [6] H. Tanaka, T. Araki, T. Koyama, and Y. Nishikawa, Universality of viscoelastic phase separation in soft matter, *J. Phys.: Condens. Matter* **17**, S3195 (2005).
- [7] I. W. Hamley, *Introduction to Soft Matter: Synthetic and Biological Self-Assembling Materials* (Wiley, Hoboken, 2007).
- [8] M. T. Connor, S. Roy, T. A. Ezquerro, and F. J. B. Calleja, Broadband ac conductivity of conductor-polymer composites, *Phys. Rev. B* **57**, 2286 (1998).
- [9] R. C. Ball and R. L. H. Essery, Surface-directed spinodal decomposition: Modelling and numerical simulations, *J. Phys.: Condens. Matter* **2**, 10303 (1990).
- [10] L. Berthier, Phase separation in a homogeneous shear flow: Morphology, growth laws, and dynamic scaling, *Phys. Rev. E* **63**, 051503 (2001).
- [11] A. A. Golovin, A. A. Nepomnyashchy, S. H. Davis, and M. A. Zaks, Convective Cahn-Hilliard Models: From Coarsening To Roughening, *Phys. Rev. Lett.* **86**, 1550 (2001).
- [12] Y. Tamura, M. Tani, and R. Kurita, Origin of nonlinear force distributions in a composite system, *Sci. Rep.* **12**, 632 (2022).
- [13] N. Nagaosa and Y. Tokura, Topological properties and dynamics of magnetic skyrmions, *Nat. Nanotechnol.* **8**, 899 (2013).
- [14] H. Mizuno, S. Mossa, and J.-L. Barrat, Relation of vibrational excitations and thermal conductivity to elastic heterogeneities in disordered solids, *Phys. Rev. B* **94**, 144303 (2016).
- [15] H. Tanaka and T. Sigehuzi, Periodic Spinodal Decomposition in a Binary Polymeric Fluid Mixture, *Phys. Rev. Lett.* **75**, 874 (1995).
- [16] S. Puri and K. Binder, Surface-directed spinodal decomposition: Phenomenology and numerical results, *Phys. Rev. A* **46**, R4487 (1992).
- [17] H. Tanaka and T. Araki, Surface effects on spinodal decomposition of incompressible binary fluid mixtures, *Europhys. Lett.* **51**, 154 (2000).
- [18] T. Araki and H. Tanaka, Hydrodynamic delocalization of phase separation in a locally cooled fluid mixture, *Europhys. Lett.* **65**, 214 (2004).
- [19] A. Krekhov, Formation of regular structures in the process of phase separation, *Phys. Rev. E* **79**, 035302(R) (2009).
- [20] A. Krekhov, V. Weith, and W. Zimmermann, Periodic structures in binary mixtures enforced by Janus particles, *Phys. Rev. E* **88**, 040302(R) (2013).
- [21] H. Furukawa, Phase separation by directional quenching and morphological transition, *Phys. A (Amsterdam, Neth.)* **180**, 128 (1992).
- [22] H. Furukawa, Concentric patterns in mesoscopic spinodal decomposition, *J. Phys. Soc. Jpn.* **63**, 3744 (1994).
- [23] B. Liu, H. Zhang, and Y. Yang, Surface enrichment effect on the morphological transitions induced by directional quenching for binary mixtures, *J. Chem. Phys.* **113**, 719 (2000).
- [24] R. Kurita, Control of pattern formation during phase separation initiated by a propagated trigger, *Sci. Rep.* **7**, 6912 (2017).
- [25] T. Tsukada and R. Kurita, Mechanism behind columnar pattern formation during directional quenching-induced phase separation, *Phys. Rev. Research* **2**, 013382 (2020).
- [26] N. Oikawa and R. Kurita, A new mechanism for dendritic pattern formation in dense systems, *Sci. Rep.* **6**, 28960 (2016).
- [27] S. Roy, S. Dietrich, and A. Maciolek, Solvent coarsening around colloids driven by temperature gradients, *Phys. Rev. E* **97**, 042603 (2018).
- [28] S. Roy and A. Maciolek, Phase separation around heated colloid in bulk and under confinement, *Soft Matter* **14**, 9326 (2018).
- [29] K. Morinaga, N. Oikawa, and R. Kurita, Emergence of different crystal morphologies using the coffee ring effect, *Sci. Rep.* **8**, 12503 (2018).
- [30] K. Morinaga, M. Tani, and R. Kurita, Formation mechanism of hierarchical structure of crystal morphology in a sessile droplet, *Phys. Rev. Research* **2**, 013098 (2020).
- [31] K. Zhang, Q. Zhang, H. Zhang, J. Shen, Q. Niu, and R. Xia, Gain properties and distributed feedback laser performance of 7f6/poly(styrene) blend films: Potential core material for plastic optical fiber expanding the bandwidth to visible region, *Macromol. Chem. Phys.* **219**, 1700527 (2018).
- [32] J. Yonemoto, Y. Maki, I. Koh, K. Furusawa, and M. Annaka, Formation of multi-channel collagen gels investigated using particle tracking microrheology, *Biomacromolecules* **22**, 3819 (2021).
- [33] M. Ginibre, S. Akamatsu, and G. Faivre, Experimental determination of the stability diagram of a lamellar eutectic growth front, *Phys. Rev. E* **56**, 780 (1997).
- [34] K. A. Jackson and J. D. Hunt, Lamellar and rod eutectic growth, *Trans. Met. Soc. AIME* **236**, 1129 (1966).
- [35] A. A. Kulkarni, J. Kohanek, K. I. Tyler, E. Hanson, D.-U. Kim, K. Thornton, and P. V. Braun, Template-directed solidification of eutectic optical materials, *Adv. Opt. Mater.* **6**, 1800071 (2018).
- [36] J.-M. Flesselles, A. J. Simon, and A. J. Libchaber, Dynamics of one-dimensional interfaces: An experimentalist's view, *Adv. Phys.* **40**, 1 (1991).

- [37] Ch.-A. Gandin, From constrained to unconstrained growth in directional solidification, *Acta Mater.* **48**, 2483 (2000).
- [38] B. Echebarria, A. Karma, and S. Gurevich, Onset of sidebranching in directional solidification, *Phys. Rev. E* **81**, 021608 (2010).
- [39] H. E. Cook, Brownian motion in spinodal decomposition, *Acta Metall.* **18**, 297 (1970).
- [40] P. K. Jaiswal, S. Puri, and K. Binder, Phase separation in thin films: Effect of temperature gradients, *Europhys. Lett.* **103**, 66003 (2013).
- [41] T. Tsukada and R. Kurita, Topological transition by confinement of a phase separating system with radial quenching, *Sci. Rep.* **9**, 15764 (2019).